A 0D stationary model for the evaluation of the degree of detachment on the divertor plates

M. Siccinio[a*], E. Fable[a], K. Lackner[a], A. Scarabosio[a], R. P. Wenninger[a,b], H. Zohm[a]

[a] *Max Planck Institut für Plasmaphysik, Boltzmannstr. 2, 85748 Garching bei München, Germany*
[b] *EUROfusion Consortium, PPPT Department, Boltzmannstr. 2, 85748 Garching bei München, Germany*

Abstract

A 0D analytical stationary model to estimate the degree of detachment on the divertor plates is derived, starting from previous works of Igitkhanov [1, 2, 3]. It accounts for heat convection, conduction, impurity radiation and contains a simplified balance for the neutrals. The upstream particle flux Γ_{up} (or, alternatively, the density upstream n_{up}), the heat flux in the scrape-off layer (SOL) q_{up} and the impurity concentrations are required as input, whereas the temperatures at the plate and at the separatrix are not fixed *a priori*. The routine has been mainly developed for system codes, or more in general for scopy studies in the framework of the preliminary design phase for the reactor DEMO, its simplicity being therefore justified by the purpose of keeping the calculation times as low as possible. A **calibration** against a more detailed 1D routine [4] has been performed, finding a reasonable agreement. Furthermore, a coupling of the model with the 1.5D transport code ASTRA [5, 6] to illustrate its possible usage is also presented.

1 Introduction

The numerous criticalities associated to the feasibility of a future nuclear fusion power plant are **related** one to the other. Thus, a comprehensive approach to the design of the prototypical machine DEMO is necessary, especially in the currently ongoing pre-conceptual design analysis phase. From this point of view, the realisation of models which are at the same time simple but able to capture the most relevant aspects of the fusion plasma physics is of primary importance. The problem of power exhaust at the divertor plates is commonly acknowledged to be a crucial issue for the design of a future nuclear fusion reactor [7]. It has already been observed [8] that, in view of the high power crossing the separatrix (around 150 MW for a conventional DEMO 1 scenario with $P_{fus} \sim 2000$ MW [9]) and of the relatively small area on which it is supposed to be deposited (according to the well-known Eich scaling [10, 11]), it would be impossible for DEMO to operate in a fully attached divertor regime without greatly exceeding the technological limit of 5-10 MW/m^2 of power exhaust on the divertor plates [12]. Thus, an at least partial detachment is

---

*Contact: mattia.siccinio@ipp.mpg.de

mandatory to be achieved in order to reduce the incoming plasma flow, and, in parallel, it is very important to develop some predictive capability to identify the conditions under which the machine can be safely operated.

In this paper, a 0D model for the estimate of the divertor detachment degree for given upstream conditions is presented. The relatively simple 0D set of equations the model consists of makes this tool particularly appropriate for being employed **as a submodule** in system codes - **i.e. codes, as for example Process [13], which identify possible operational points for fusion reactors satisfying at the same time physical, technological and economical constraints -** , or more in general for the search of optimised design points on a power plant level. In spite of its unavoidably simplistic approach, justified by the aim of keeping the computational time as low as possible in view of a coupling with more comprehensive design softwares, the model embraces the prominent physical mechanisms determining the onset of detachment (heat convection, heat conduction, impurity radiation, ionisation and charge exchange), possessing therefore a high flexibility together with a reasonable degree of accuracy.

The paper is structured as follows: in section 2, the equations are derived and presented, in section 3 the validation of the model by means of a more detailed 1D routine (developed by Kallenbach *et al.* and in turn validated against experimental data of ASDEX Upgrade, see [4]) is discussed. Section 4 contains an exemplary application of the tool, which has been coupled with the 1.5D transport code ASTRA [5, 6] to investigate the efficiency of different impurity mixings, whereas conclusions are drawn in section 5.

2   The Model

A magnetic field line (*rectius*, a flux tube) of length $L_\parallel$ which connects the outer midplane to the divertor plate is artificially subdivided into two regions, labelled with I and II. More specifically:

- **Region I**. Therein, the heat is supposed to be transported along the field line only via *conduction*, whereas the static pressure is supposed to be constant. Impurity radiation is present, and the relative concentration of the radiative species is supposed to be spacially homogeneous. The region extends from the outer midplane for a distance indicated with L_r, which is an output of the model.

- **Region II**. This is the *convective* region, which starts from L_r and reaches the target plate. It is characterised by pure convection (assuming Mach number $M = 1$), constant total pressure and impurity radiation, with the relative concentration of the radiative species again supposed to be homogeneous. Its length is denoted with $L_m = L_\parallel - L_r$. The transition between conduction and convection is supposed to take place where
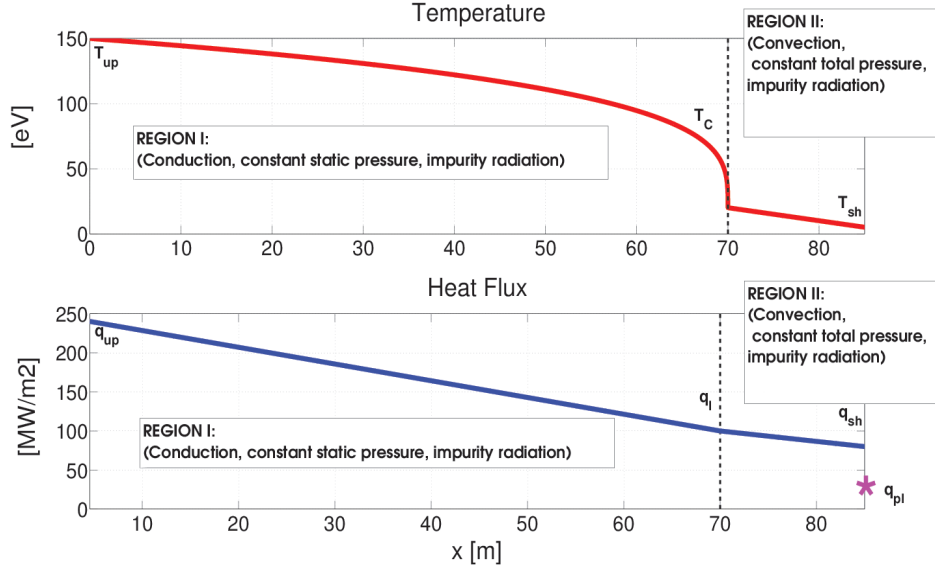
Figure 1: Schematic representation of the field line between outer midplane and target plate. The difference between q_{sh} and q_{pl} **(indicated by the magenta star)** is due both to momentum losses, that reduce the particle flux, **and to the purely geometrical effect of the inclination of the tiles with respect to the magnetic field line (q_{pl} has the meaning of heat flux perpendicular to the target plates, thus it is not defined on the flux tube cross section)** . The vertical dashed line has been set at $x = L_r$ to identify the boundary between the conductive and the convective region. The temperature and $q_{\parallel}$ profiles represented here are purely illustrative.

a critical temperature T_C, which is a free parameter in the model, is reached. The choice of identifying the transition between conduction and convection by means of a critical temperature is connected to the fact that, for very high q_{up}, low temperatures are typically reached when a large fraction of the power entering the SOL is radiated, so that the convective transport can carry a significant fraction of the residual flux. This approach might however be questionable in a scenario with reduced energy losses, where low temperatures could be reached simply because of the high gradients necessary to sustain the heat conduction.

The temperature at the plates, indicated with T_{sh}, acts as input for the momentum loss calculation, discussed below. In order to keep the model simple enough, the interaction with the neutrals is assumed not to massively affect the heat transport and the temperature profiles, which are therefore calculated at constant total plasma pressure. In the following, quantities defined at the outer midplane are denoted by the subscript up and quantities at the interface be-

tween the conductive and the convective region with the subscript I. A further distinction is introduced between quantities defined at the end of the magnetic fieldline *but without having considered momentum losses* , indicated with sh, and quantities actually reaching the target plate after the interaction with the neutrals, indicated with the subscript pl. **In this simple 0D limit, this interaction with the neutrals is supposed to take place punctually at the target plate, although in reality this is obviously a volumetric phenomenon. Furthermore, the calculation of q_{pl} takes into account the inclination of the magnetic field line with respect to the divertor tiles (q_{pl}, as a matter of fact, has the meaning of heat flux perpendicular to the target plates rather than of parallel heat flux). It is here stressed that the variations of the cross section along the flux tube, due for example to the variations in the strength of B [14] and which change the value of $q_{\parallel}$, having therefore repercussions on the temperature profile, have not been included at this stage.** Fig.1 schematically depicts the subdivision of the magnetic field line.

Analogously to the well-known two-point-model [15], it is here supposed that the entire particle and energy flux crossing the separatrix be concentrated at the outer midplane. In principle, region I could be understood as the "scrape-off layer" region (hencefort SOL), whereas the **convective** region represents the "divertor" region. *Such identification is however somehow misleading, because the transition between the two regions is not supposed to be located at a precise position along the field line, but it moves according to the temperature profile.* In particular, if the temperature remains above T_C everywhere, L_r coincides with $L_{\parallel}$ and no convective region is considered at all, although, obviously, the divertor is still present. In the following, a description of the equations in the model is given.

2.1 Density Upstream

The model has as an input the particle flux at the separatrix. However, what enters the successive equations is rather the density n_{up}. To connect the two quantities, a radial density profile which decays exponentially outside the separatrix at the outer midplane is assumed, namely

$$n(r) = n_{up} \exp\left(-\frac{r}{\lambda_p}\right) \tag{1}$$

(with $r = 0$ identifying the separatrix), together with a diffusive ansatz across the magnetic field lines

$$\Gamma_{up} = -D_r \left.\frac{\mathrm{d}n}{\mathrm{d}r}\right|_{r=0}. \tag{2}$$

Putting the two equations together, one finds

$$n_{up} = \lambda_p \frac{\Gamma_{up}}{D_r} \tag{3}$$

The value of the two parameters λ_p and D_r has to be prescribed by the user. Reasonable values are $\lambda_p = 5$ mm or more, $D_r = 1$ m^2/sec, or less [16]. The use of Eq.3 can be avoided if the value of n_{up} is known.

2.2 Region I

The equations for the conductive region are derived from two 1D equations plus one boundary condition, which are subsequently manipulated to obtain a set of 0D equations. The heat flux $q(x)$ (x being the coordinate along the field line, $x = 0$ identifying the outer midplane and $x = L_\parallel$ corresponding to the target plate) is supposed to be transported purely via conduction, namely

$$q(x) = -\chi_0 T(x)^{5/2} \frac{\mathrm{d}T(x)}{\mathrm{d}x}, \tag{4}$$

with $T(x)$ the local temperature (we assume ion and electron temperatures to be everywhere equal) and $\chi_0 T^{5/2}$ representing the well-known Spitzer-Härm conductivity (with $\chi_0 = 2390$ W/m eV$^{7/2}$). Impurity radiation lets the heat flux vary along the field line,

$$\frac{\mathrm{d}q(x)}{\mathrm{d}x} = -n(x)^2 c_z^I l_z(T) \tag{5}$$

where c_z^I is the (constant) fraction of impurities with respect to the electron density $n(x)$, while l_z is the cooling factor. These equations can be combined and then integrated, leading to

$$q(T)^2 = q_I^2 + 2\chi_0 (n_{up} T_{up})^2 c_z^I \int_{T_C}^{T} \mathrm{d}T \sqrt{T} l_z(T), \tag{6}$$

having exploited the constancy of the static pressure, i.e. $n(x)T(x) = n_{up}T_{up}$. This equation, originally derived by Lengyel [17], for $T = T_{up}$ reads

$$q_{up}^2 = q_I^2 + 2\chi_0 (n_{up} T_{up})^2 c_z^I \int_{T_C}^{T_{up}} \mathrm{d}T \sqrt{T} l_z(T). \tag{7}$$

The second equation directly descends from of Eq.4. Observing that the heat flux depends on x only through the temperature, it is possible to write

$$\mathrm{d}x = -\chi_0 T^{5/2} \frac{\mathrm{d}T}{q(T)}. \tag{8}$$

Integrating on the length of the conductive domain, one finds

$$L_r = \chi_0 \int_{T_C}^{T_{up}} \mathrm{d}T \frac{T^{5/2}}{q(T)}, \tag{9}$$

where $q(T)$ is known from Eq.6. The last equation corresponds to the purely conductive boundary condition at the interface between region I and II, assuming constant total pressure, Mach number $M = 1$ (these two conditions together

5

leading to $n_{up}T_{up} = 2n_{sh}T_{sh}$) and having introduced the sheath multiplication factor γ **(i.e. the widely employed numerical factor connecting the heat load removed at the divertor plates to the local plasma density and temperature, see e.g. [16])**,

$$q_I = \frac{\gamma}{2}en_{up}T_{up}c_{s0}\sqrt{T_C}. \tag{10}$$

Here, e indicates the electron charge, m_i the ion mass, and $c_{s0} = \sqrt{2e/m_i}$ is the sound speed calculated at $T_{ref} = 1$ eV (thus $c_{s0}\sqrt{T}$ is the sound speed at temperature T). **The use of γ (which is a quantity defined at the sheath) at the interface between region I and II is discussed in the next subsection.** The three unknowns are q_I, T_{up} and L_r. If no convective region is present (i.e. no solution with $L_r < L_\parallel$ can be found), the transition temperature T_C (known) is substituted by T_{sh} (unknown), whereas L_r (unknown) is set equal to $L_\parallel$ (known), leaving otherwise the equations unchanged.

2.3 Region II

In the convective region, the equation for q_{sh} is derived on the same footing of **Eq.7**, accounting for the radiation losses - contrarily to what happened in the original Igitkhanov model [1, 2, 3], where divertor radiation was not considered. Starting point is the impurity radiation equation Eq.5, again assuming constant total pressure and $M = 1$,

$$\frac{\mathrm{d}q(x)}{\mathrm{d}x} = -\frac{n_{up}^2 T_{up}^2}{4}c_z^{II}\frac{l_z(T)}{T(x)^2} \tag{11}$$

together with the equation for the convected power (which in our assumptions coincides with the total power)

$$q(x) = \frac{\gamma}{2}en_{up}T_{up}c_{s0}\sqrt{T(x)}. \tag{12}$$

Eq.12 can be derived with respect to x and then substituted into Eq.11. Employing straightforward algebra, one finds

$$\int_{T_{sh}}^{T_C}\mathrm{d}T\frac{T^{3/2}}{l_z(T)} = \frac{n_{up}T_{up}c_z^{II}}{\gamma ec_{s0}}L_m \tag{13}$$

The model is closed by the boundary condition at the plate

$$q_{sh} = \frac{\gamma}{2}en_{up}T_{up}c_{s0}\sqrt{T_{sh}}. \tag{14}$$

Eq.13 and 14 are employed to determine the two unknowns T_{sh} and q_{sh}. **The fact that the sheath multiplication factor γ must be used at the transition between region I and II and throughout region II (see Eq.10 and 12) is required to enforce consistency in the limit of no radiating impurities. In such limit, in fact, one should recover $T_{sh} = T_C$ because of the pure convection assumption, $n_{sh} = n_I$ for the constancy of the pressure and $q_{sh} = q_I$ for the energy conservation.**
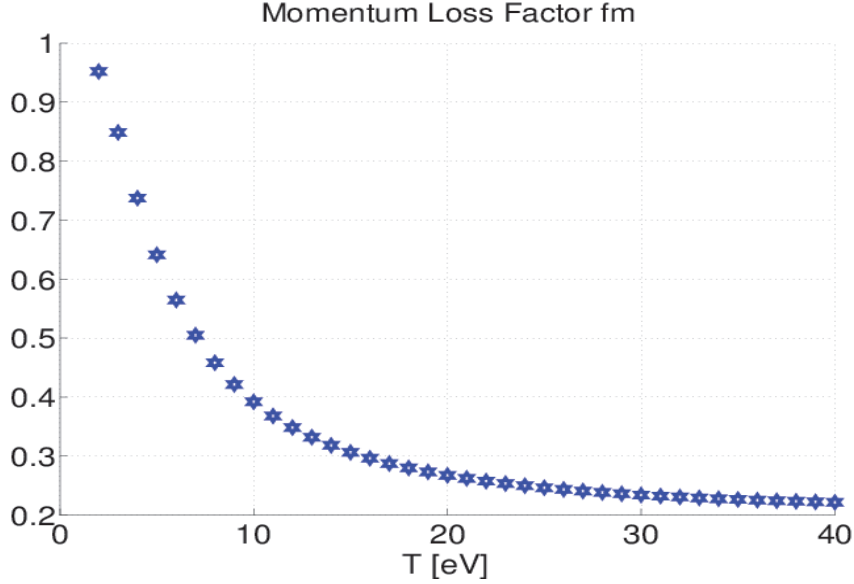
6

Figure 2: Momentum loss factor f_m as a function of the temperature according to Eq.17.

2.4 Neutrals and Divertor Detachment

For the momentum loss due to the interaction of the neutrals with the incoming plasma flow, we employ a very simple model taken from the literature (originally developed by Self and Ewald [18], it has been included in the comprehensive review by Pitcher and Stangeby [19]). This model is based on the competition between charge exchange and ionisation, which mainly depends on the plasma temperature T_{sh}. It is herewith stressed that, in principle, *every* model for the neutrals requiring in input only T_{sh} can be implemented at this point, this providing our tool a certain degree of flexibility. Estimating φ - the ratio between the ionisation and the charge exchange cross sections - with [20]

$$\varphi = 2.8 \frac{\exp\left(-13.6/T_{sh}\right) T_{sh}^{0.19}}{6 + 0.073 T_{sh}}, \tag{15}$$

where T_{sh} has to be provided in eV, one introduces the dimensionless parameter α_{ps}

$$\alpha_{ps} = \frac{\varphi}{1 + \varphi}. \tag{16}$$

The momentum loss factor f_m - defined as the ratio between the total pressure losses and the total pressure upstream - is calculated as [18, 19]

$$f_m = 1 - 2 \left(\frac{\alpha_{ps}}{1 + \alpha_{ps}}\right)^{(\alpha_{ps}+1)/2}. \tag{17}$$

7

The corresponding thermal flux at the plates reads then

$$q_{pl} = (1 - f_m)\frac{q_{sh}}{\eta_{\mathbf{B}}} = (1 - f_m)\frac{\gamma}{2\eta_{\mathbf{B}}}en_{up}T_{up}c_{s0}\sqrt{T_{sh}}, \tag{18}$$

where $\eta_{\mathbf{B}}$ is the factor which accounts for the **inclination of the magnetic field line w.r.t. the divertor tiles** (other variations in the flux tube cross section along the field line are not accounted for, **as previously mentioned**). The momentum loss factor f_m is employed in the model as the measure of the detachment degree. In particular, $f_m = 0$ corresponds to a fully attached situation, whereas $f_m = 1$ corresponds to a vanishing flux on the target plate. The usual definition of degree of detachment Γ, i.e. the ratio between the "ideal" flux calculated by means of the two-point model and the actual flux, is recovered as

$$\Gamma = \frac{1}{1 - f_m}. \tag{19}$$

Fig.2 shows f_m as a function of the temperature according to Eq.15-17.

2.5 Overview

The model consists of eight equations and eight unknowns (n_{up}, T_{up}, q_I, L_r, T_{sh}, q_{sh}, f_m, q_{pl}), which reduce to six in the purely conductive case (as $q_I = q_{sh}$ and $L_r = L_\parallel$). **Incidentally, it is observed that the quantity f_m only depends on T_{sh}, thus the corresponding equation, and subsequently the one for q_{pl}, are actually decoupled from the system of equations.** The upstream power flux q_{up}, the upstream particle flux Γ_{up} and the impurity concentrations are required as input. For convenience, we re-write the entire system of equations here:

$$n_{up} = \lambda_p \frac{\Gamma_{up}}{D_r} \tag{20}$$

$$q_{up}^2 = q_I^2 + 2\chi_0(n_{up}T_{up})^2 c_z^I \int_{T_C}^{T_{up}} dT\sqrt{T}l_z(T) \tag{21}$$

$$L_r = \chi_0 \int_{T_C}^{T_{up}} dT\frac{T^{5/2}}{q(T)} \tag{22}$$

$$q_I = \frac{\gamma}{2}en_{up}T_{up}c_{s0}\sqrt{T_C} \tag{23}$$

$$\int_{T_{sh}}^{T_C} dT\frac{T^{3/2}}{l_z(T)} = \frac{n_{up}T_{up}c_z^{II}}{\gamma ec_{s0}}L_m \tag{24}$$

$$q_{sh} = \frac{\gamma}{2}en_{up}T_{up}c_{s0}\sqrt{T_{sh}} \tag{25}$$

$$f_m = 1 - 2\left(\frac{\alpha_{ps}}{1 + \alpha_{ps}}\right)^{(\alpha_{ps}+1)/2} \tag{26}$$

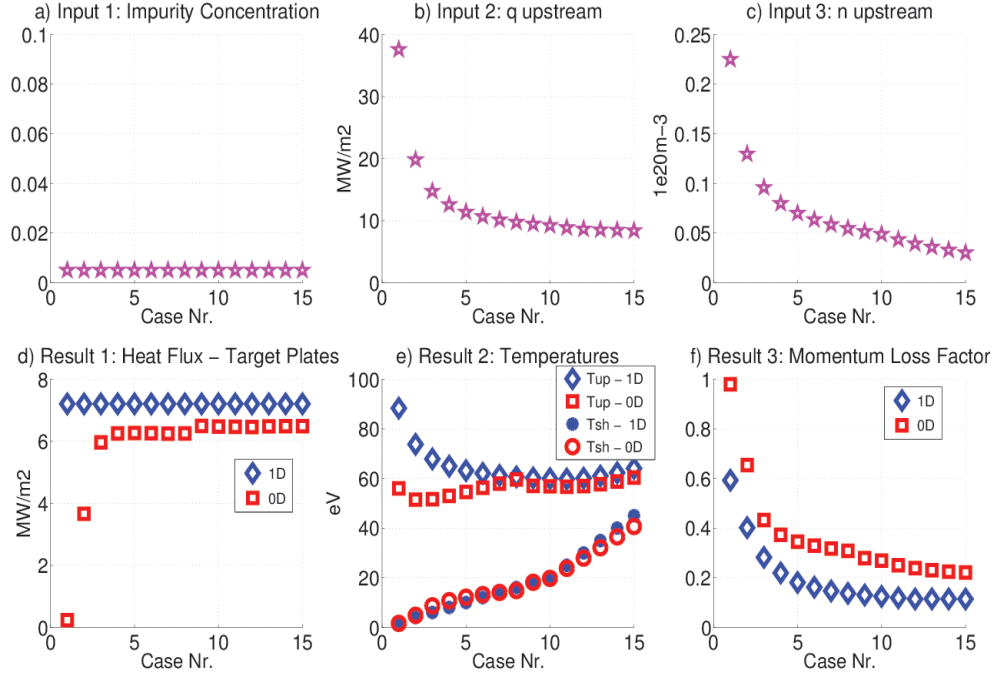$$q_{pl} = (1 - f_m)\frac{\gamma}{2\eta_{\mathbf{B}}}en_{up}T_{up}c_{s0}\sqrt{T_{sh}}, \tag{27}$$

8

Figure 3: Results of the calibration - low impurity concentration case (for $\gamma = 9.2$ and $T_C = 15$ eV). The power at the target for the 1D code has been fixed to 0.6 MW, the nitrogen relative concentration amounts to 0.5% and a scan in T_{sh} has been performed. Plots a), b) and c) show the input quantities for the 0D model ($c_z^I = c_z^{II}$, q_{up} and n_{up}, respectively), whereas plots c), d) and e) compare the 0D model output quantities (q_{pl}, T_{up}, T_{sh} and f_m) to the corresponding quantities from the 1D calculations. Blue symbols identify 1D results, red symbols 0D results.

where $q(T)$ in Eq.22 is given by Eq.6. A multi-species generalisation of the model (i.e. considering more than one radiative atomic species at once) is straightforward. Indicating with $c_{z,j}^I$, $c_{z,j}^{II}$ and $l_{z,j}(T)$ the concentrations and
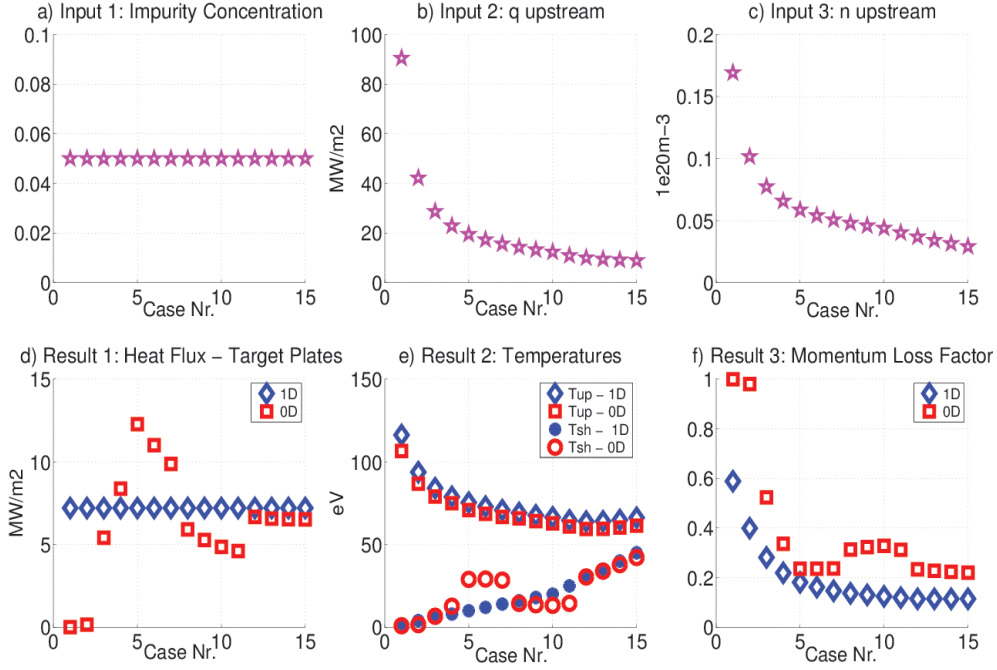
Figure 4: Results of the calibration - high impurity concentration case **(for $\gamma = 9.2$ and $T_C = 15$ eV)**. The power at the target for the 1D code has been fixed to **0.6** MW, the nitrogen relative concentration amounts to 5% and a scan in T_{sh} has been performed. Plots a), b) and c) show the input quantities for the 0D model ($c_z^I = c_z^{II}$, q_{up} and n_{up}, respectively), whereas plots c), d) and e) compare the 0D model output quantities (q_{pl}, T_{up}, T_{sh} and f_m) to the corresponding quantities from the 1D calculations. Blue symbols identify 1D results, red symbols 0D results.

the cooling factor of the j-th species, the system Eq.20-27 takes the form

$$n_{up} = \lambda_p \frac{\Gamma_{up}}{D_r} \tag{28}$$

$$q_{up}^2 = q_I^2 + 2\chi_0(n_{up}T_{up})^2 \sum_j c_{z,j}^I \int_{T_C}^{T_{up}} dT \sqrt{T} l_{z,j}(T) \tag{29}$$

$$L_r = \chi_0 \int_{T_C}^{T_{up}} dT \frac{T^{5/2}}{q(T)} \tag{30}$$

$$q_I = \frac{\gamma}{2} e n_{up} T_{up} c_{s0} \sqrt{T_C} \tag{31}$$

$$\int_{T_{sh}}^{T_C} dT \frac{T^{3/2}}{\sum_j c_{z,j}^{II} l_{z,j}(T)} = \frac{n_{up}T_{up}}{\gamma e c_{s0}} L_m \tag{32}$$

$$q_{sh} = \frac{\gamma}{2} e n_{up} T_{up} c_{s0} \sqrt{T_{sh}} \tag{33}$$

$$f_m = 1 - 2 \left(\frac{\alpha_{ps}}{1 + \alpha_{ps}} \right)^{(\alpha_{ps}+1)/2} \tag{34}$$

$$q_{pl} = (1 - f_m) \frac{\gamma}{2\eta_{\mathbf{B}}} e n_{up} T_{up} c_{s0} \sqrt{T_{sh}}. \tag{35}$$

The free parameters for the calibration are basically two: T_C and γ. Also, the impurity radiation data can be corrected by means of a numerical factor. The **calibration** against a more sophisticated 1D code is discussed in the next section.

3   Calibration

The code against which the **calibration** has been performed is the 1D code developed recently by Kallenbach et al [4]. This code solves the continuity, momentum and energy conservation equations for the plasma and a simplified continuity equation for the neutrals along a magnetic field line, thus yielding parallel profiles of densities, velocities and temperatures. As input, it needs power and temperature at the divertor plates - equations are so to say solved "backwards", contrarily to the 0D routine presented here. In order to carry out the **calibration**, one has therefore to run a 1D calculation fixing T_{sh} and P_{Target}, subsequently employing the calculated n_{up} and q_{up} as input for the 0D routine and then comparing the two results. The impurity radiation data - only one species, nitrogen, has been employed - have been taken from ADAS [**21**], assuming a non-coronal parameter $n_e \tau = 0.5$ ms 1e20m^{-3}. The connection length of the considered field line has been set to $L_{\parallel} = 120$ m. Two different scans in T_{sh} (from $T_{sh} = 2$ eV to $T_{sh} = 45$ eV) with P_{Target} fixed at **0.6 MW** for different impurity concentrations have been performed (the relatively low value of P_{Target} has been chosen in order to reach low temperatures, where the most interesting physical phenomena take place, without employing unrealistically high values for n_{up}). Incidentally, note that varying T_{sh} for fixed P_{Target} also implies a modification in n_{up} and q_{up}, as can be seen in Fig.3 b) and c), as well as in Fig.4 b) and c). **The best agreement with the 1D routine has been obtained setting $\gamma = 9.2$ and $T_C = 15$ eV in the 0D routine**, the latter value being essentially consistent with recent experimental observations [22]. The impurity radiation for the conductive region has been corrected with a factor 0.4. The need for such correction is probably due to the fact that, in reality, no "strong" separation between conductive and convective regions exists and therefore, even in a conduction dominated regime, a temperature gradient still survives, weakening the effect of the radiative cooling (this point will be addressed in future releases of the model). **Fig.3 and Fig.4 show the comparison of the calibrated model against the 1D calculations. In particular,** Fig.3 shows the results for a nitrogen concentration of 0.5%. As one can see, the agreement on the temperatures is quite good, especially for T_{sh} - which is the most important parameter for the estimate of the detachment degree. The onset of the detachment (i.e. the variation of the slope in the f_m curve) starts to take place at around 3-5 eV (in agreement with [20]). A second test has been carried out with a higher impurity concentration - 5% - in order to verify the model under more challenging conditions (as the impurity concentration increases, the difference between a 0D and a 1D routine able to reproduce the temperature profiles is expected to become more significant).

The results are shown in Fig.4. Again, the agreement is quite good, although not as good as before for the reason just elucidated. Nevertheless, the onset of detachment is again quite well reproduced, the errors on T_{sh} being mostly relevant in the non-detached, high T_{sh} cases. **The fact that the Self-Ewald model overestimates f_m in comparison to the 1D calculations, Fig.3 f) and Fig.4 f), explains the underestimate of q_{pl} at very low temperatures, see Fig.3 d), Fig.4 d) and Eq.18. A better determination of the momentum loss factor as a function of T_{sh} is left for future work.**
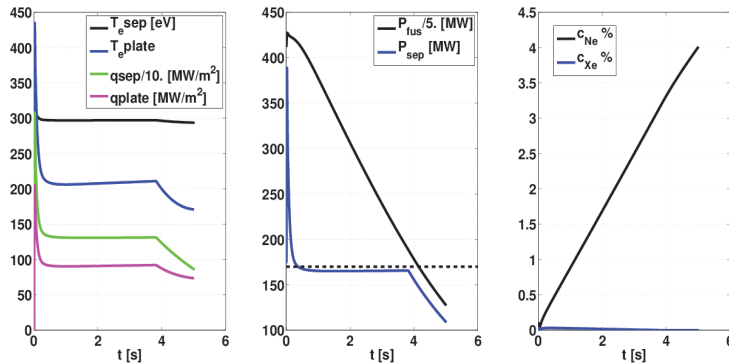
Figure 5: ASTRA Results: Xe-Ne case. The first figure shows the time evolution of the heat fluxes and the temperatures at the outer midplane and on the divertor plate, the second one shows the time evolution of the generated fusion power and of the corresponding P_{SOL}, whereas the third one contains the time evolution of the impurity concentrations in the core. **In this case, no stationary solution satisfying the constraints could be found and the simulation was interrupted at $t = 5$ s.**

4   Applications

In this section, an exemplificative application of the model is presented. The routine has been coupled with the well-known core transport code ASTRA [5, 6] to carry out a preliminary DEMO investigation (in particular, the chosen reference case is a DEMO 1 scenario with $P_{fus} = 2$ GW [9]). ASTRA calculates the density and temperature profiles in the core plasma for a DEMO equilibrium, providing to the 0D routine the required particle flux and the heat flux at the separatrix (more correctly, ASTRA calculates the power at the separatrix P_{SOL}, which is then converted in the parallel flux q_{up} employing the well known expression

$$q_{up} = \frac{P_{SOL}}{2\pi R \lambda_q \frac{B_{pol}}{B_{tor}}}, \tag{36}$$

where the e-folding length λ_q has been set to the value of 1 cm, R is the major radius and B_{pol} and B_{tor} are the poloidal and toroidal component of the
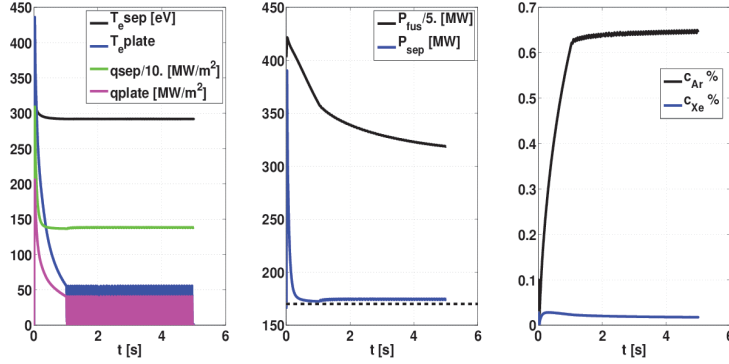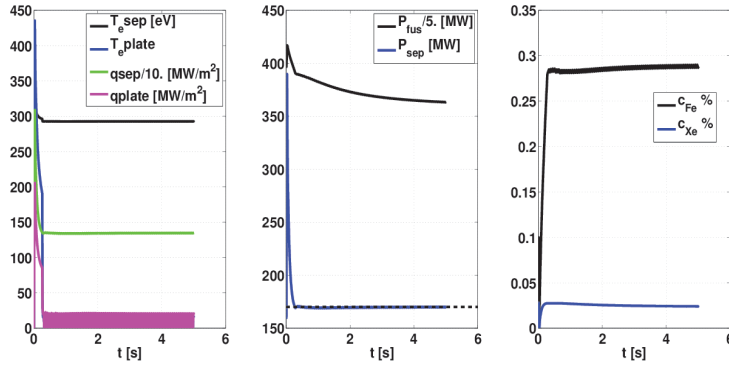
Figure 6: ASTRA Results: Xe-Ar case. The first figure shows the time evolution of the heat fluxes and the temperatures at the outer midplane and on the divertor plate, the second one shows the time evolution of the generated fusion power and of the corresponding P_{SOL}, whereas the third one contains the time evolution of the impurity concentrations in the core. **A stationary solution satisfying the constraints has been found. The meaning of the oscillations is discussed in the main text.**

Figure 7: ASTRA Results: Xe-Fe case. The first figure shows the time evolution of the heat fluxes and the temperatures at the outer midplane and on the divertor plate, the second one shows the time evolution of the generated fusion power and of the corresponding P_{SOL}, whereas the third one contains the time evolution of the impurity concentrations in the core. **A stationary solution satisfying the constraints has been found. The meaning of the oscillations is discussed in the main text.**

magnetic field at the outer midplane, respectively). The multi-species version of the model (Eq.28-35), with the calibration data determined in the previous section (i.e. $T_C = 15$ eV, $\gamma = 9.2$ and a radiation correction factor for the conductive region of 0.4) has been employed. The noble gas xenon, which is
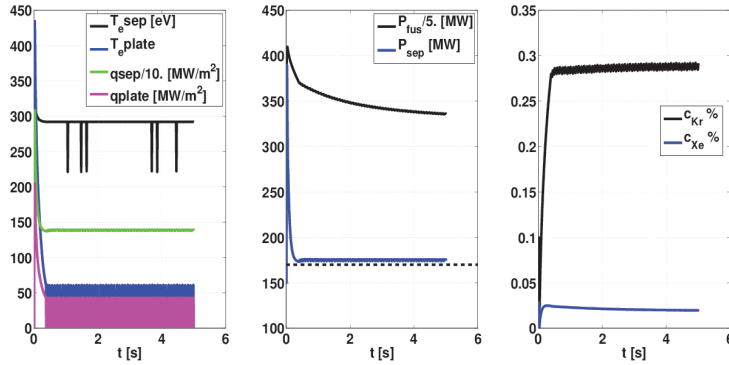
13

Figure 8: ASTRA Results: Xe-Kr case. The first figure shows the time evolution of the heat fluxes and the temperatures at the outer midplane and on the divertor plate, the second one shows the time evolution of the generated fusion power and of the corresponding P_{SOL}, whereas the third one contains the time evolution of the impurity concentrations in the core. **A stationary solution satisfying the constraints has been found. The meaning of the oscillations is discussed in the main text.**
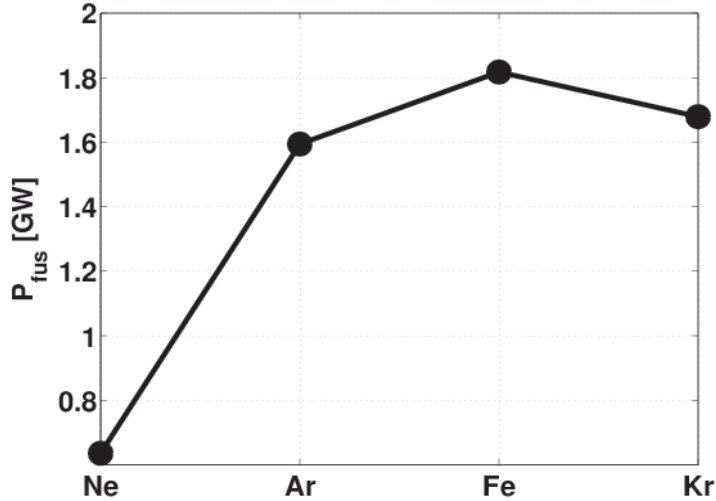

Figure 9: ASTRA Results: Final value of the fusion power as a function of the chosen SOL radiating impurity.

supposed to play the role of main radiative species for the plasma core (recall that the reactor DEMO is supposed to radiate a fraction of the alpha power of around 75% in the core [7, 9]) is **paired with** a second atomic species j, which
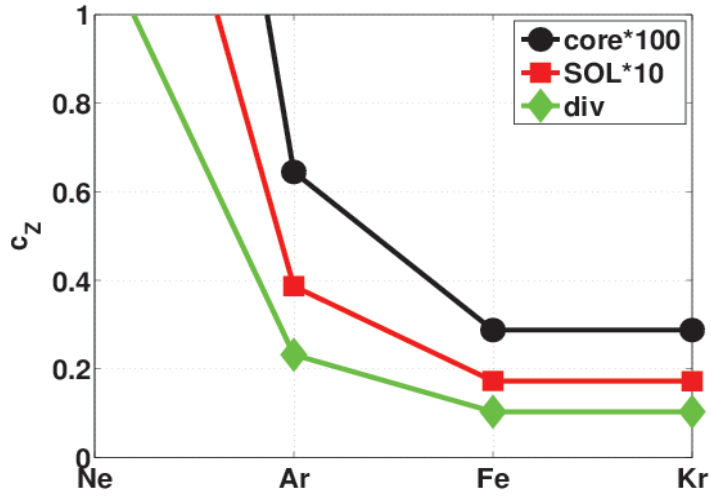
14

Figure 10: ASTRA Results: Final value of the SOL radiating impurity concentration as a function of the chosen SOL radiating impurity.
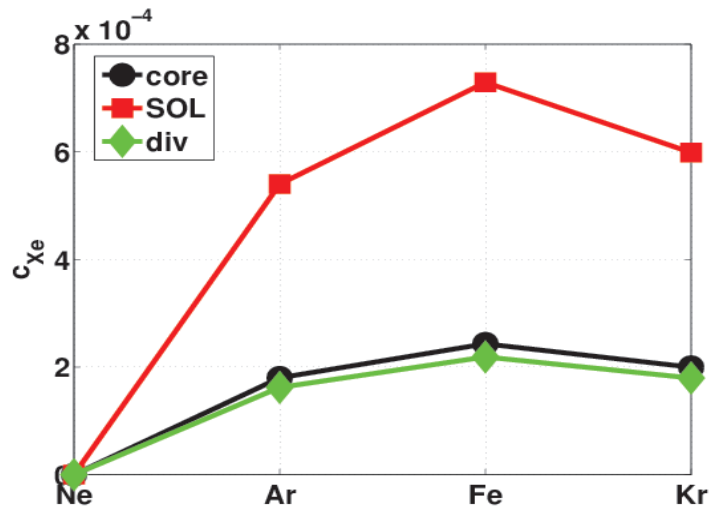

Figure 11: ASTRA Results: Final value of the Xe concentration as a function of the chosen SOL radiating impurity.

is on the contrary employed to radiate in the SOL/divertor. Xenon is supposed to be puffed at the outer midplane, its concentration in region I, $c_{z,XE}^I$, being therefore connected to its core concentration in a simplified way by means of a

constant peaking factor $w_{Core,I}^{Xe}$

$$w_{Core,I}^{Xe} \doteq \frac{c_{z,Xe}^{Core}}{c_{z,Xe}^{I}}, \tag{37}$$

which has been set to the value of 0.3. Similarly, a peaking factor between region I and II,

$$w_{II,I}^{Xe} \doteq \frac{c_{z,Xe}^{II}}{c_{z,Xe}^{I}}, \tag{38}$$

has been set to the value of 0.3 (this means, in other words, that the Xe concentrations in the core and in the divertor are supposed to be almost equal to one third of the SOL one, where the gas is puffed). The second atomic species j is on the contrary supposed to be puffed directly in the divertor, being therefore more concentrated in region II than in region I or in the core. Specifically, the values

$$w_{Core,I}^{j} \doteq \frac{c_{z,j}^{Core}}{c_{z,j}^{I}} = 0.15 \tag{39}$$

and

$$w_{II,I}^{j} \doteq \frac{c_{z,j}^{II}}{c_{z,j}^{I}} = 6 \tag{40}$$

have been set. Clearly, the question whether these peaking factors are possible to be achieved in reality with each of the considered j-impurities goes beyond the goals of the present analysis. In view of what was already mentioned in section 1, it is also important to repeat that *when the temperature is everywhere larger than T_C, region II is not taken into account in the calculation, and subsequently the value c_z^{II} has no impact at all on the result*. Again, this is due to the fact that the correspondance between region II and divertor volume shall not be understood in a strictly geometrical sense.

For the second species j, four options have been considered in the present analysis, namely argon, neon, krypton and iron. ASTRA dynamically calculates the density, temperature and fusion power profiles in the core, providing new values of q_{up} and n_{up} to the 0D model, which in turn determines q_{pl}, and dynamically changes the impurity concentrations until the constraints of $P_{SOL} \geq 170$ MW (**i.e. above the predicted value necessary for the L-H transition, see [9]**) and $q_{pl} \leq 10$ MW/m^2 (**i.e. below the technological limit for the divertor plates [12]**) are simultaneously fulfilled. **More in detail, the Xe concentration (recall that xenon is here employed as radiative species for the core) is modified according to the value of P_{SOL} - if $P_{SOL} > 170$ MW, then the Xe concentration is increased, and reduced otherwise. On the same footing, the concentration of the j-th impurity species (Ne, Fe, Kr, Ar) is set according to the value of q_{pl} - if $q_{pl} > 10$ MW/m^2, the concentration is increased and decreased otherwise. It is also assumed that concentrations can be**

changed instantaneously in the plasma, this occurrence being obviously not realistic, a more careful analysis of the impurity transport going however beyond the purposes of such exemplificative applications of the model. The scheme according to which impurity concentrations are changed is not meant to be a control scheme, but rather a scheme for the search of steady state solutions satisfying the above criteria. In view of the peaking factors, it is impossible to change the SOL radiation without affecting the main plasma and viceversa, therefore ASTRA repeats the calculation of the core profiles any time the concentrations are varied. *The goal of this investigation consists in determing which impurity combination is able to fulfill the requirements on P_{SOL} and q_{pl} having at the same time the smallest impact on the performance of the reactor*, which essentially means keeping the fusion power at an acceptable level.

The results of the calculations are shown in Fig.5-11. In Fig.5, one can observe that it has been impossible for ASTRA to find a stationary solution with neon. In fact, a strong deterioration in the fusion power takes places before having achieved a sufficient reduction of the heat flux at the target plate. This because, in spite of the quite low value of $w^j_{Core,I}$, the neon concentration in the main plasma dilutes the core too much in comparison to the little benefits in the SOL. The simulation has been interrupted at $P_{SOL} \simeq 110$ MW, as its continuation would simply have led to a further reduction of the fusion power. On the contrary, a solution has been found for argon, krypton and iron. Observing Fig.6-8, one can notice that the T_{sh} and q_{pl} curves start to violently oscillate after a sufficiently low temperature is reached. This is a consequence of the fact that, when $T_{sh} < T_C$, the **convective** region - which has an impurity concentration $c^{II}_{z,j} \sim 36$ times larger than the core region - comes suddenly into play, dramatically enhancing the radiated power. ASTRA reacts back by correcting the impurity concentration, but this small correction is sufficient to increase T_{sh} above T_C again, this entire sequence leading to the observed oscillating behaviour without however significantly affecting the value of P_{SOL}. These sudden jumps in the radiative power could be avoided by means of a non-stationary version of the model, including a more detailed description of the impurity transport, which is however left for future work. Such oscillating regime can be understood as the onset of the detachment, or in other words the final values of the impurity concentrations identify possible DEMO operational points which satisfy the required constraints (the final value of P_{fus} is contained in Fig.9, whereas final concentrations for xenon and for the considered SOL radiative species are shown in Fig.10 and 11, respectively). Interestingly, the best reactor performance has been achieved with iron, which has however the obvious drawback of not being a gas and therefore being impossible to be puffed. Although these calculations are to some extent simplistic, this analysis shows that the performance of a nuclear fusion reactor is crucially connected to the possibility of achieving high impurity concentrations in the SOL without deathly affecting the core.

5   Summary and Conclusions

We have developed a 0D, stationary model for the calculation of the divertor detachment onset to be employed in system codes or in general for integrated modelling purposes. The presented model is able to reproduce with a satisfactory accuracy the results of a more detailed 1D code while keeping the calculation times much faster. In particular, the temperature at the plates, which represents the key parameter to identify the onset of the detachment, seems to be correctly reproduced. We think that the routine presented here possesses all the necessary features to be employed in the preliminary design of a nuclear fusion reactor like DEMO, as the ASTRA calculations presented in section 4 show. For future work, a more extensive calibration campaign against SOLPS and against experimental data, together with the development of a non-stationary version of the model possibly including a more detailed treatment of impurity transport, are planned.

6   Acknowledgments

References

[1] Yu. Igitkhanov *et al.*, 21st EPS, Montpellier, ECA v.18B, 1994

[2] Yu. Igitkhanov *et al.*, 22th EPS, Bournemouth, ECA v.19C, 1995

[3] Yu. Igitkhanov, KIT Scientific Reports 7661 (2014)

[4] A. Kallenbach *et al.*, Plasma Phys. Control. Fusion **58**, 045013 (2016)

[5] G. V. Pereverzev, IPP Report 5/42 (1991)

[6] E. Fable *et al.*, Plasma Phys. Control. Fusion **55**, 124028 (2013)

[7] H. Zohm *et al.*, Nucl. Fusion **53**, 073019 (2013)

[8] R. P. Wenninger *et al.*, Nucl. Fusion **54**, 114003 (2014)

[9] G. Giruzzi *et al.*, Nucl. Fusion **55**, 073002 (2015)

[10] T. Eich *et al.*, Phys. Rev. Lett. **107**, 215001 (2011)

[11] T. Eich *et al.*, Nucl. Fusion **53**, 093031 (2013)

[12] **G. Federici** *et al.***, Fusion Eng. Des. 89 Issue 7-8, 882 (2014)**

[13] **M. Kovari** *et al.***, Fusion Eng. and Des. 89, 3054 (2014)**

[14] **I. H. Hutchinson, Nucl. Fusion 34, 1337 (1994)**

[15] M. Keilhacker. Plasma Physics and Controlled Nuclear Fusion Research, III:183 (1982)

[16] P. C. Stangeby, The Plasma Boundary of Magnetic Fusion Devices, ISBN-10: 0750305592

[17] L. L. Lengyel, IPP Report 1/191 (1981)

[18] S. A. Self and H. N. Ewald, Phys. Fluids **9**, 2486 (1966)

[19] C. S. Pitcher and P. C. Stangeby, Plasma Phys. Control. Fusion **39**, 779 (1997)

[20] K. Lackner *et. al*, WPDTT1 - CD02 (unpublished) 2015

[21] **ADAS manual and documentation 2016 www.adas.ac.uk/manual.php**

[22] A. Leonard *et al.*, Nucl. Fusion **52**, 063015 (2012)